

Quantitative Evaluation of the Interaction Between Wear and Corrosion on Mg-3Gd-1Zn Alloy in Simulated Body Fluid

Xiaobo Zhang, Jianwei Dai, Jie Zhang, and Yunqiang Bai

(Submitted May 11, 2018; in revised form October 9, 2018; published online November 26, 2018)

As potential temporary implants, biodegradable magnesium (Mg) alloys will undergo fretting friction and corrosion simultaneously in human body. Aiming at illustrating the interaction between wear and corrosion of Mg alloys, wear and corrosion rates in simulated body fluid (SBF) were quantitatively evaluated on Mg-3Gd-1Zn (wt.%, GZ31) alloy. Wear behaviors of the alloy in SBF were compared with those under dry sliding condition, and corrosion rates of the alloy accompanied with wear were also compared with those without wear in SBF. The characteristic parameters of wear tracks were collected by 3D surface profile. The results indicated that the friction coefficient in SBF was much lower as compared to that under dry sliding condition. Owing to the protection of Mg(OH)₂ and lubrication of SBF, wear was significantly restricted, but due to the galvanic corrosion between matrix and wear debris, corrosion was seriously aggravated. Most of the mass loss was attributed to corrosion rather than wear for the wear test in SBF.

Keywords biomaterial, corrosion and wear, magnesium

1. Introduction

Owing to good biodegradation, biocompatibility, mechanical and physical properties (Ref 1-3), Mg alloys have become the most promising metallic materials in orthopedic implants, the representative examples of which are bone plates and screws (Ref 4-7). Biodegradable Mg alloys play an important impermanent role in providing adequate strength in service and then degrade completely after they finish supporting or connecting tasks (Ref 8-10).

Fretting and corrosion may occur at the interfaces between human bone and implants (Ref 11, 12). The keel failure caused by the aseptic loosening may be essentially owing to the wear debris and corrosion particles (Ref 12). And it is suspected that the bone screws would suffer from wear during the initial implanting process. Tribocorrosion was also detected at the contacting interfaces between the implants subject to minute relative movements according to the studies (Ref 13-16). Recent study has found that the nitinol spinal rods were sensitive to fretting corrosion on the surfaces in conjunction with titanium pedicle screws (Ref 13). In general, the fretting and corrosion behaviors are unavoidable due to the service condition in human body, which would accelerate failure of implants, including titanium alloys and stainless steels currently used in clinic (Ref 17-20). It has been indicated that peripros-

thetic bone loss would be caused owing to the presence of particulate wear products surrounding the implant (Ref 21). Compared with these traditional metallic bone plates and bone screws, biodegradable Mg alloys exhibit poor corrosion resistance and may cause more complex synergistic effects (Ref 10). However, there have been few studies on the interaction between wear and corrosion of biodegradable Mg alloys. Li (Ref 22) and Liu (Ref 23) qualitatively pointed out that the corrosion effect of Mg-Zn-Ca alloy and Mg-2Zn-0.2Mn alloy in SBF was more dominant than its lubrication effect during the process of friction. Semblable phenomena were also detected in Mg-Zn-Zr alloy (Ref 24) and Mg-Gd-Zn-Zr alloy (Ref 25). In general, the present studies of these synergistic effects on biodegradable Mg alloys mainly concentrated on qualitatively assessing mass loss caused by wear and corrosion, but not quantitatively.

Therefore, in this work, Mg-3Gd-1Zn (wt.%, GZ31) alloy with good corrosion resistance in SBF (Ref 26) was selected as the research alloy and the mass loss of the alloy in SBF severally caused by wear and corrosion was distinguished. The actual volume loss only caused by wear in SBF condition was characterized by 3D profiler, and wear rates under SBF condition were calculated. As a result, mass loss rates caused by wear and corrosion have been quantitatively distinguished under SBF condition. Furthermore, the interaction between wear and corrosion was discussed.

2. Materials and Methods

2.1 Sample Preparation

The as-cast Mg-3Gd-1Zn (wt.%, GZ31) ingots were prepared by gravity casting process (Ref 26). Specimens with dimension of 10 mm × 10 mm × 6 mm were cut by wire cut electrical discharge machining. After grinding by 1200 grit SiC

Xiaobo Zhang, Jianwei Dai, and Yunqiang Bai, School of Materials Engineering, Nanjing Institute of Technology, Nanjing 211167, China; and Jiangsu Key Laboratory of Advanced Structural Materials and Application Technology, Nanjing 211167, China; Jie Zhang, School of Materials Engineering, Nanjing Institute of Technology, Nanjing 211167, China. Contact e-mail: xbxzhang2003@163.com.

paper, they were polished, cleaned with ultrasonic cleaner, and dried.

2.2 Microstructure and Phase Characterization

Microstructure was examined by a scanning electron microscope (SEM, Carl Zeiss Merlin Compact) equipped with an energy-dispersive spectrometer (EDS, Atec X-max 50). Phase identification was conducted by x-ray diffraction (XRD, Ultima-IV). The scanning rate was 6°/min, and the 2θ ranged from 20° to 80°.

2.3 Immersion Test

Immersion test was performed at 37 °C in SBF (Ref 23). The mass of the samples was weighed prior to immersion, which was marked as M_1 . Then, the specimens after 180 min immersion were cleaned in a 200 g/L CrO₃ solution for 5 min to remove corrosion products and then weighed again, marked as M_2 . The immersion mass loss rate of the alloy was calculated by the following formula (Ref 27):

$$V_{\text{corr}} = \frac{M_2 - M_1}{AT} \quad (\text{Eq 1})$$

where V_{corr} is the corrosion rate (mg/(min cm²)), M_1 and M_2 are the mass mentioned above (mg), A is the surface area of the specimen (cm²) and T is the immersion time (min).

2.4 Wear Test and 3D Profiler Scanning

Wear tests under dry and SBF conditions (Fig. 1) were carried out on a ball-on-disk wear testing machine (Rtec MFT-3000) at room temperature. Taking stress range of surgical implants into consideration, specimens were tested under normal applied load of 5 N, sliding speed of 30 mm/s, stroke length of 2 mm and sliding time of 10, 20, 60, and 180 min, respectively (Ref 9, 17, 18). The mass of the samples prior to and following wear test was weighed. For dry sliding test, the samples were ultrasonically cleaned in ethanol to remove wear

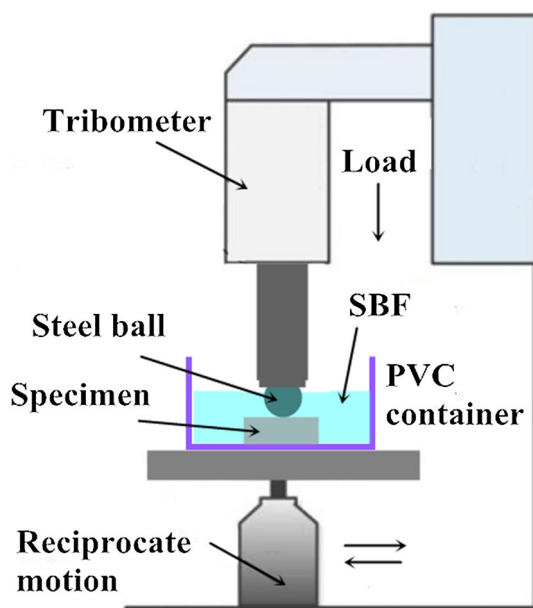


Fig. 1 Schematic diagram of the platform for friction and wear test in SBF

debris. For the samples tested in SBF, they were weighed again after removing corrosion products as the same way of cleaning immersion samples. Worn morphologies and wear debris were observed by SEM, and chemical compositions were analyzed by EDS.

The wear rates of the alloys were calculated by the following formula (Ref 28):

$$V_{\text{wear}} = \frac{\Delta m}{FL} \quad (\text{Eq 2})$$

where V_{wear} is the wear mass loss rate (g/N m), Δm is the mass loss (g), F is the applied load (N), and L is the total sliding distance (m).

Wear tracks were scanned by 3D profiler (VHX-1000), which could record the contour line of the tracks' cross section and the corresponding coordinates. On the one hand, the wear track's cross-sectional area was calculated in infinitesimal method by these coordinates. The volume loss caused by wear was calculated, and then it was converted into mass loss. The actual wear rates in SBF were calculated through formula (2). On the other hand, the mass loss caused by corrosion was acquired by using total mass loss minus mass loss caused by wear, and then corrosion rates in SBF condition were obtained through formula (1). This method distinguished the actual mass loss produced by wear in SBF from the total mass loss caused by both wear and corrosion.

3. Results and Discussion

3.1 Matrix Characterization

Figure 2(a) shows SEM micrograph of the as-cast GZ31 alloy. The microstructure is composed of α -Mg matrix, eutectic phase (as indicated by 1 in Fig. 2a) discontinuously located at the grain boundaries and lamellar structure (as indicated by 2 in Fig. 2a). The lamellar structure in Mg-Gd-Zn(-Ca, Zr, Mn) alloys was characterized as long-period stacking ordered structure or its initial stage (stacking faults) (Ref 26, 29). The XRD pattern in Fig. 2(b) reveals that both α -Mg and (Mg,Zn)₃Gd phases are detected. As a result, the eutectic phase along the grain boundaries is (Mg,Zn)₃Gd.

The mass loss in SBF caused only by corrosion was obtained by immersion test in order to compare with that accompanied by wear. The corrosion rate is 9.66×10^{-4} mg/(min cm²) following 180 min immersion.

3.2 Wear Morphologies and Wear Debris Analysis

The micrographs in Fig. 3 show the worn surfaces under different conditions after 10 and 180 min wear test. The worn area under dry sliding condition is much larger than that under SBF condition for the same test time. And the larger width and depth values of the wear track collected by 3D profiler obviously prove the SEM morphologies, as presented in Fig. 3(e) and (f). The wear track of the alloy as well as the corresponding contour line of the tracks' cross section in SBF is much smoother than that under dry sliding condition, suggesting good lubrication of SBF.

The blocks in Fig. 3(b) indicate the corrosion products accumulated on two marginal edges of the track and more aggregated corrosion products distributed on the surfaces (marked by arrows in Fig. 3d). This suggests that corrosion

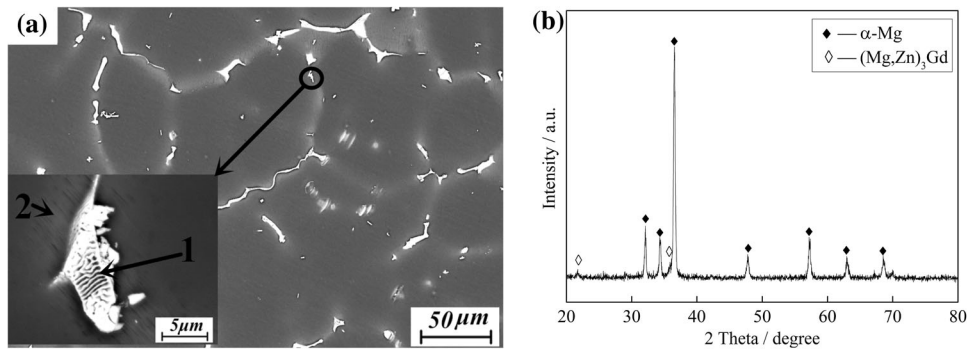


Fig. 2 SEM micrograph (a) and XRD spectrum (b) of GZ31 alloy

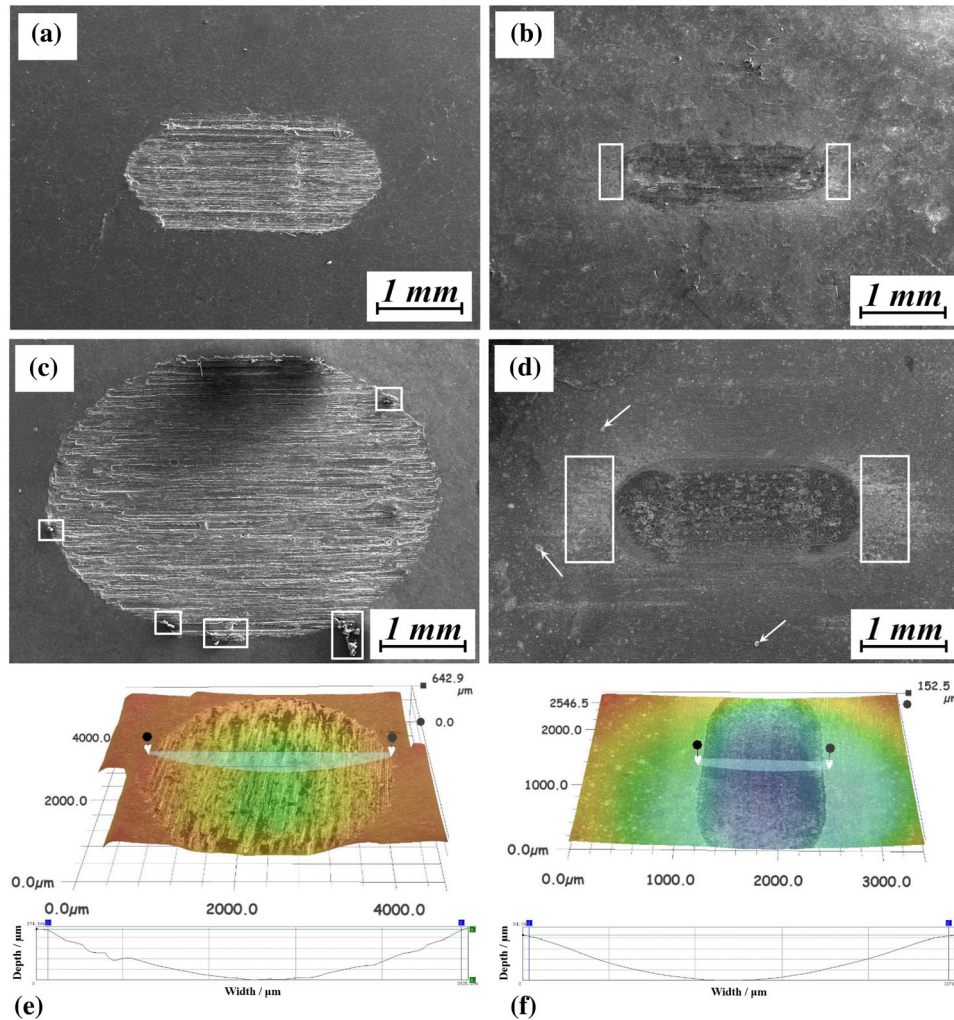


Fig. 3 Macrographs of the worn surfaces under dry sliding condition (a, c) and SBF condition (b, d) tested for 10 min (a, b) and 180 min (c, d); accompanying with wear tracks and the corresponding contour line of the tracks' cross section under dry sliding condition (e) and SBF condition (f) tested for 180 min

of the surface around the wear track was accelerated, which may be ascribed to the occurrence of galvanic corrosion between matrix and wear debris. With the increase of sliding time, the width of track under dry condition becomes wider, as well as the length. However, the track area in SBF condition does not change too much with prolonging test time.

Figure 4 presents the high-magnification micrographs of the worn surfaces under different conditions for 10 and 180 min, respectively. As shown in Fig. 4(a) and (b), there are numerous long grooves parallel to the sliding condition with some flattened bright particles, manifesting obvious abrasion and oxidation (Ref 30-33). The grooves following 10 min wear in SBF are much slighter as compared to those under drying

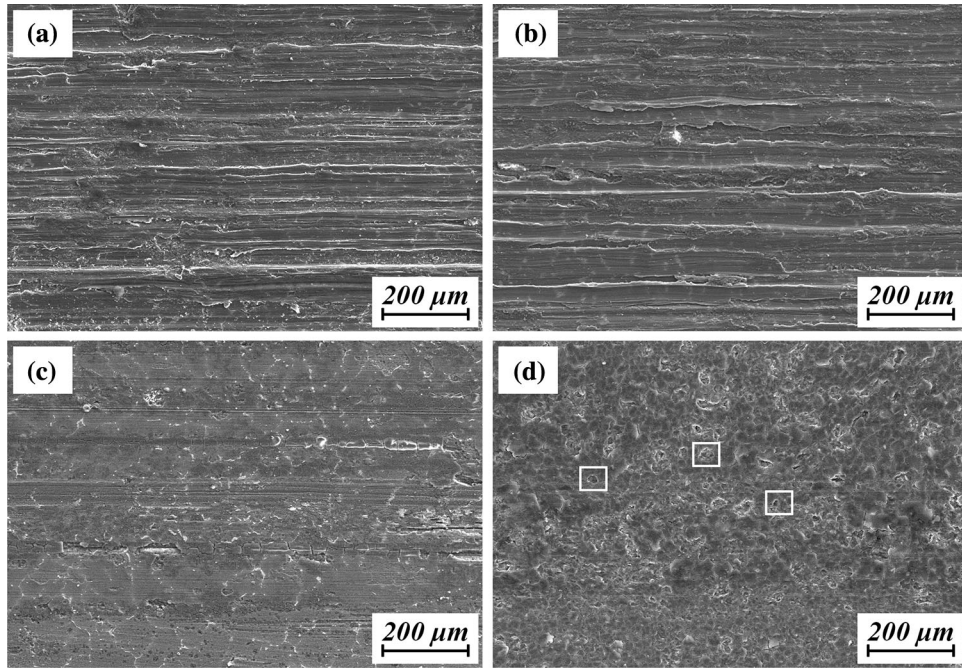


Fig. 4 High-magnification SEM micrographs of the worn surfaces under dry sliding condition (a, b) and SBF condition (c, d) following 10 min (a, c) and 180 min (b, d) tests

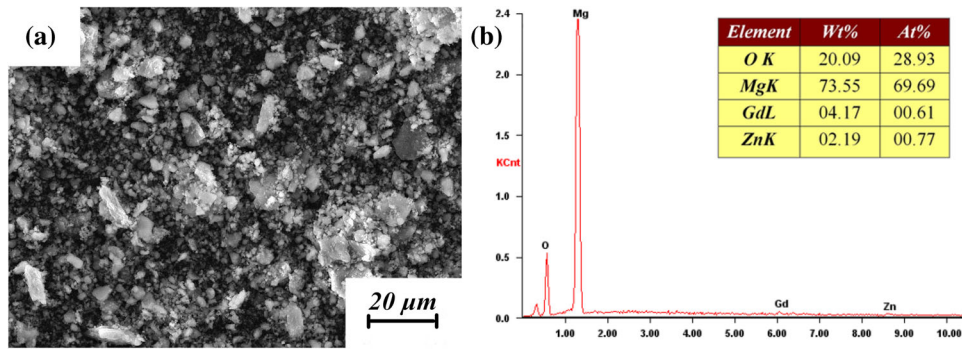


Fig. 5 SEM micrographs of the wear debris under dry sliding for 180 min (a) and its EDS spectrum (b)

condition. With prolonging test time, the grooves are even invisible, and more corroded pits are formed, as shown in Fig. 4(d), indicating the change from abrasive to corrosive wear (Ref 34, 35).

The wear debris morphologies and compositions under dry sliding condition for 180 min are presented in Fig. 5. It can be observed that the debris are in different sizes and shapes, including tiny grainy and large flakes. EDS results show that the debris are rich in Mg and O, along with a little Gd and Zn. These data suggest that abrasion and oxidation dominate the wear mechanisms under dry sliding condition. The wear debris in SBF is not available because of the difficulty in collection.

3.3 Wear-Resistant Properties

The average friction coefficient under SBF and dry sliding conditions is presented in Fig. 6. It can be detected that the values in both conditions generally present increased trend with the increase of sliding time, and the friction coefficient curve in

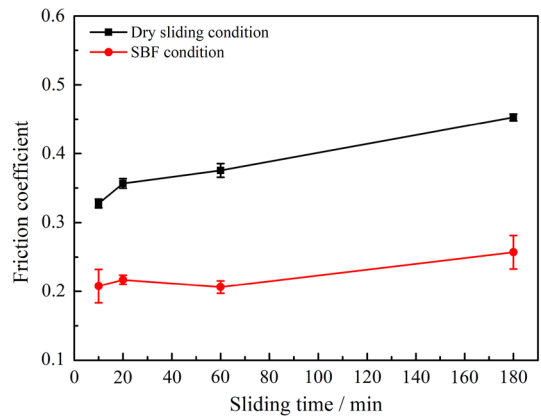


Fig. 6 Average friction coefficient versus the sliding time under SBF and dry sliding condition

SBF is obviously lower than that under dry sliding condition, verifying good lubrication of SBF.

Figure 7 demonstrates the relationship of total mass loss under dry sliding and SBF conditions. The mass loss under both conditions is very close after 10 min wear test; however, the mass loss in SBF is higher than that under dry sliding condition following 20, 60, and 180 min wear test. What is noteworthy is that the mass loss in dry condition only comes from wear, while the mass loss in the SBF condition stems from wear and corrosion. According to Fig. 3, it is clear that the worn tracks in SBF are much smaller than those under dry sliding condition following the same test time, which means that the mass loss caused by wear in SBF is much less than that under dry sliding condition. As a consequence, mass loss caused by corrosion is responsible for the even higher total mass loss in SBF as compared to that under dry sliding condition.

In order to verify the reliability of the calculating method through 3D profiler, the wear volume acquired by 3D profiler method and the wear volume calculated by mass loss method are presented in Fig. 8. It indicates that the values came from 3D profiler and mass loss methods do not make obvious difference: The wear volume obtained by 3D profiler method is slightly higher (< 20%) than that by mass loss under dry sliding condition for the same test time, which proves the relative dependability of 3D profiler method. Therefore, the

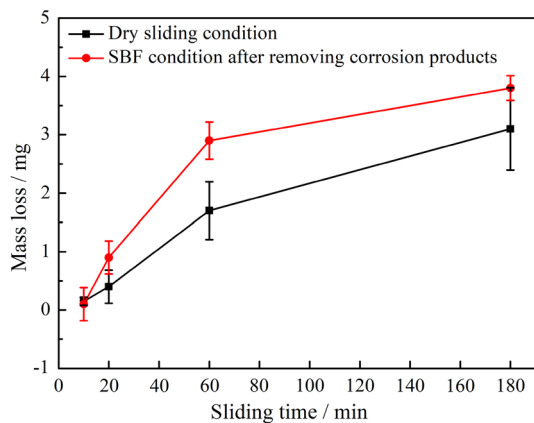


Fig. 7 Total mass loss versus the sliding time under dry sliding condition and SBF condition (after removing corrosion products)

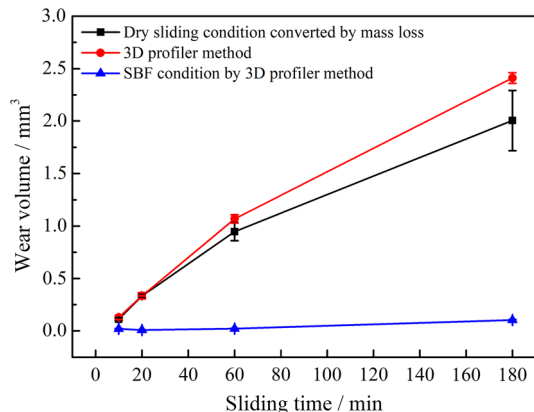


Fig. 8 Wear volume under SBF and dry sliding conditions

wear volume in SBF obtained by 3D profiler method is reliable. Volumes of the worn tracks in SBF calculated by 3D profiler method are also shown in Fig. 8. The wear volumes in SBF are much lower than those under dry sliding. With increasing sliding time, the former increases slightly while the latter increases obviously, representing that the mass loss only caused by wear in SBF is much lower than that under dry sliding condition, which corresponds well with the results shown in Fig. 3.

Figure 9 presents the proportion of mass loss caused by wear versus the sliding time under SBF condition. It has been observed that the values of the percentage are no more than 5% except the value for 10 min sliding (35%). It demonstrates that most of the mass loss is attributed to corrosion but not wear in SBF, particularly with prolonging test time; in other words, corrosion has more influence on the total mass loss of the as-cast GZ31 alloy under SBF condition than wear.

The actual corrosion mass loss in SBF with and without wear is presented in Fig. 10(a). The mass loss values in immersion test without wear are only caused by corrosion, and they are calculated by the average corrosion rate following 180 min immersion test since even the total mass loss is relatively low. It can be detected that the corrosion mass loss in SBF accompanied with wear after 10 min test was close to that without wear, and then it is much higher than that without wear with prolonging sliding time. The mass loss in SBF with wear is over 1.9, 13.5, 14.5, and 6.1 times higher as compared to that without wear after 10, 20, 60, and 180 min test. This result indicates that wear apparently aggravates corrosion in SBF, and the degree of aggravation is intensified first and then reduced with the increase of sliding time.

The wear rates under both conditions are shown in Fig. 10(b). The variation tendency shows that the wear rates are much lower in SBF than those under dry sliding condition. The wear rate in SBF is 23.6, 4.0, 2.7, and 5.9% of that under dry sliding condition after each sliding time. These results indicate that wear is effectively restricted in SBF.

3.4 Discussion

Mg alloys corrode easily in chloride ions environment, such as SBF condition. Usually, $Mg(OH)_2$ film is easily formed on the surface of Mg alloys in SBF at the initial stage that will protect matrix from corrosion. With the increase of immersion time, the film will convert into soluble $MgCl_2$ with the

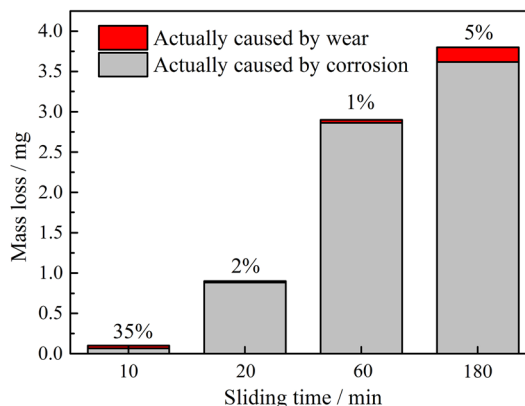


Fig. 9 Mass loss percentage of the alloy caused by wear and corrosion separately in SBF

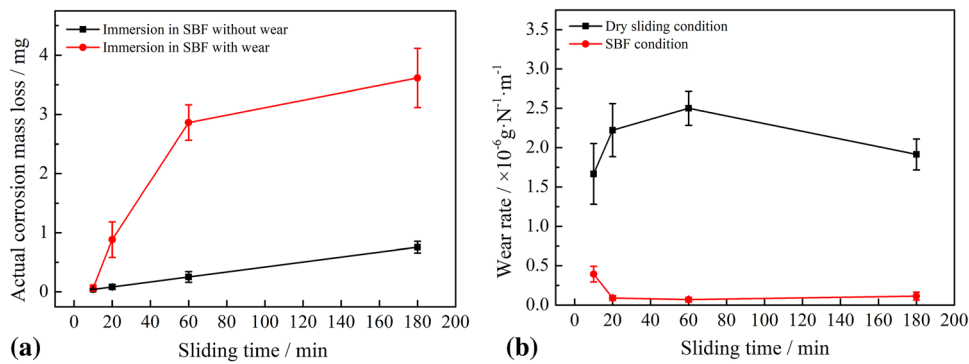


Fig. 10 Actual corrosion mass loss for immersion and wear tests in SBF (a) and wear rates under dry sliding and SBF conditions (b)

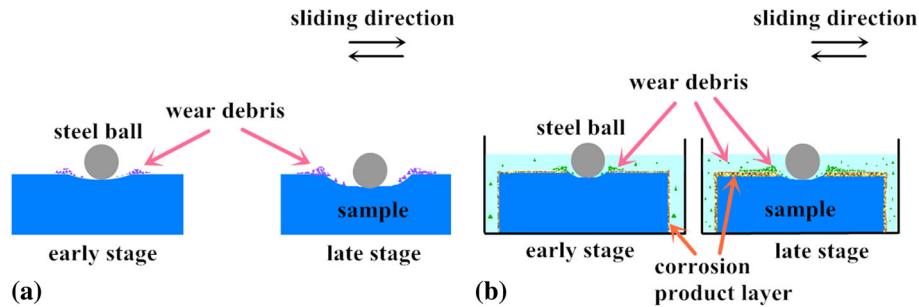


Fig. 11 Schematic diagram of synergistic effects happening in the as-cast Mg-3Gd-1Zn alloy under dry sliding (a) and SBF conditions (b)

accumulation of Cl^- , which cannot play protective role as effectively as $\text{Mg}(\text{OH})_2$ (Ref 36). Friction coefficient is mainly influenced by surface roughness and hardness of the matrix. For the wear test in SBF, $\text{Mg}(\text{OH})_2$ film was formed on the worn surface and it has insufficient time to transform into soluble MgCl_2 because of cyclic friction. The friction coefficient is low and corrosive wear dominates the wear process. Contrarily, more grooves (as shown in Fig. 4a and b) have been detected under dry sliding condition, and abrasive wear and oxidation wear are the main wear mechanisms. Consequently, the friction coefficient values under dry sliding condition are higher than those in SBF. Moreover, the increased friction coefficient under dry sliding condition is mainly attributed to the softening of the specimen caused by friction heat and larger contact surface with prolonging sliding time (Ref 37); however, the increased contact surface leads to the slight friction coefficient increase in SBF.

In the dry sliding test, the mass loss is only produced by wear, whereas the mass loss for the wear test in SBF comes from both wear and corrosion. Figure 9 indicates that corrosion effect accounts for much more part in the total mass loss than wear effect. Figure 10(a) reveals that the corrosion rates in SBF for wear test are much higher as compared to those for immersion test, and Fig. 10(b) demonstrates that the wear rates in SBF are much lower than those in dry sliding state. In brief, wear was significantly inhibited in SBF while corrosion was severely accelerated by wear.

Figure 3(b) and (d) indicates that the corrosion product particles are distributed on surface of the specimen because of the introduction of wear; moreover, the electrochemical reaction between the Mg alloys and the counter-face of the steel ball may also accelerate corrosion (Ref 25). As a result, the total

mass loss in SBF is even higher than that under dry sliding though the actual wear volume is much less, as shown in Fig. 7 and 8. Due to the lubrication of the SBF and the protection of $\text{Mg}(\text{OH})_2$ film, wear was effectively restricted. Generally, it is concluded that corrosion effect has more effect on the total mass loss than the wear effect under SBF condition. Similar synergistic effect was also detected in other Mg alloys (Ref 23-25, 37, 38).

In this work, it is noted that the synergistic effect between wear and corrosion in SBF has been quantitatively evaluated. The mass loss caused by wear in SBF accounts for only 35, 2, 1, and 5%, respectively, following 10, 20, 60, and 180 min test, and the rest mass loss is ascribed to corrosion. The wear rate in SBF is 23.6, 4.0, 2.7, and 5.9% of that under dry sliding condition after 10, 20, 60, and 180 min wear test. The mass loss by corrosion in SBF with wear is over 1.9, 13.5, 14.5, and 6.1 times higher as compared to that without wear after each time parameter. These results infer that even the wear rate of the alloy will be apparently reduced in SBF; nevertheless, the corrosion will be accelerated severely by the wear. Therefore, as for the implants served under unavoidable fretting friction condition, the wear resistance is one of the important properties to be taken into account.

Figure 11 shows the schematic diagram of Mg alloy sample under SBF and dry sliding conditions in different stages. Under dry sliding condition, with the prolonging sliding time, more wear debris were produced and heaped around the wear track, particularly at both ends of the wear track. A few of them were embedded into matrix and were not cleaned off completely, as denoted in Fig. 3(c). The width and depth of the track also increased, as shown in Fig. 11(a). It corresponded with the increasing trend of actual wear volume under dry sliding

condition in Fig. 3 and 8. Under SBF condition, most wear debris were washed to both terminals by SBF. The surface around the wear track suffered severe corrosion due to the galvanic corrosion between wear debris and matrix, as shown in Fig. 3(b) and (d). The other surfaces underwent less corrosion than the surfaces near the wear track because of little dissociative wear debris in SBF. With the increase of sliding time, this galvanic corrosion effect apparently increased first and then showed a decreasing trend because of thicker corroded layer on the sample surface. Because of the protective Mg(OH)₂ film and lubricative SBF solution, the width and depth did not increase as quickly as those under dry sliding, and the wear rates were much lower.

Comparing the sample in two conditions, although the total mass loss is similar, it is obvious that the mass loss in dry sliding condition simply comes from wear, and the mass loss in SBF condition is mainly caused by corrosion. The wear mechanism in SBF is corrosive wear and those under dry sliding condition are abrasion and oxidation. It is noticeable that for the benefit of SBF, wear is restricted prominently; however, wear directly deteriorates corrosion and thus accelerates the total mass loss of the sample, and thus, the impact of wear in SBF cannot be neglected.

4. Conclusions

To figure out the quantitative interaction between wear and corrosion on GZ31 alloy, experiments including immersion test, sliding test under dry and SBF conditions were conducted. The main conclusions are summarized as follows:

1. The average friction coefficient in SBF condition is lower than that in dry sliding state due to Mg(OH)₂ film and lubrication caused by SBF.
2. The mass loss caused by wear in SBF accounts for 1–35%, and the rest is ascribed to corrosion for the experiments.
3. Wear is significantly impeded by SBF, and the wear rate in SBF ranges from 2.7 to 23.6% of that under dry sliding condition.
4. The corrosion is worsened by 6.1 times by wear after 180 min test, which is mainly due to the galvanic corrosion caused by wear debris.
5. Wear not only results in mass loss itself, but also speeds up corrosion. Hence, it is of great significance to pay more attention on wear effect of Mg alloys for biomedical applications.

Acknowledgments

This project was supported by the Natural Science Foundation of Jiangsu Province for Outstanding Youth (BK20160081), the Innovative Foundation Project for Students of Nanjing Institute of Technology (TP20170011, TB201816036), the Six Talent Peaks (2015-XCL-025) of Jiangsu Province, and Innovation Foundation of Nanjing Institute of Technology (CKJB201302), and the Outstanding Scientific and Technological Innovation Team in Colleges and Universities of Jiangsu Province.

References

1. Y.J. Chen, Z.G. Xu, C. Smith, and J. Sankar, Recent Advances on the Development of Magnesium Alloys for Biodegradable Implants, *Acta Biomater.*, 2014, **10**, p 4561–4573
2. K.K.A. Kumar, U.T.S. Pillai, B.C. Pai, and M. Chakraborty, Dry Sliding Wear Behavior of Mg-Si Alloys, *Wear*, 2013, **303**, p 56–64
3. N. Li and Y.F. Zheng, Novel Magnesium Alloys Developed for Biomedical Application: A Review, *J. Mater. Sci. Technol.*, 2013, **29**, p 489–502
4. J. Zhang, X.B. Zhang, Q.H. Liu, S.J. Yang, and Z.Z. Wang, Effects of Load on Dry Sliding Wear Behavior of Mg-Gd-Zn-Zr Alloys, *J. Mater. Sci. Technol.*, 2017, **33**, p 645–651
5. D.W. Zhao, F. Witte, F.Q. Lu, J.L. Wang, J.L. Li, and L. Qin, Current Status on Clinical Applications of Magnesium-Based Orthopaedic Implants: A Review from Clinical Translational Perspective, *Biomaterials*, 2017, **112**, p 287–302
6. X.D. Kong, L. Wang, G.Y. Li, X.H. Qu, J.L. Niu, T.T. Tang, K.R. Dai, G.Y. Yuan, and Y.Q. Hao, Mg-Based Bone Implants Show Promising Osteoinductivity and Controllable Degradation: A Long-Term Study in a Goat Femoral Condyle Fracture Model, *Mater. Sci. Eng. C*, 2018, **86**, p 42–47
7. J. Zhou, M.L. Zhou, J. Zheng, and T. He, Study of the Anti-Corrosion and Anti-Fretting Properties of Surficial Treated Magnesium Alloy Bone Plate, *CH. J. Med. Instr.*, 2016, **40**, p 347–350
8. J.W. Dai, X.B. Zhang, and Z.Z. Wang, Microstructure and Enhanced Corrosion Resistance of Biodegradable Mg-Gd-Cu-Zr Alloy by Solution Treatment, *Mater. Technol.*, 2018, **33**, p 301–310
9. M.A. Hussein, A.S. Mohammed, and N. Al-Aqeeli, Wear Characteristics of Metallic Biomaterials: A Review, *Materials*, 2015, **8**, p 2749–2768
10. X.G. Sun, M. Nouri, Y. Wang, and D.Y. Li, Corrosive Wear Resistance of Mg-Al-Zn Alloys with Alloyed Yttrium, *Wear*, 2013, **302**, p 1624–1632
11. C. Wan, Z.X. Hao, and S.Z. Wen, Research and Prospect on the Fretting Tribology of the Orthopedic Implants, *Tribology*, 2012, **32**, p 102–112
12. C. Kajetanek, B. Bouyer, M. Ollivier, P. Boisrenoult, N. Pujol, and P. Beaufils, Mid-Term Survivorship of Mini-Keel™ Versus Standard Keel in Total Knee Replacements: Differences in the Rate of Revision for Aseptic Loosening, *Orthop. Traumatol. Surg. Res.*, 2016, **102**, p 611–617
13. E. Lukina, M. Kollerov, J. Meswania, A. Khon, P. Panin, and G.W. Blunn, Fretting Corrosion Behavior of Nitinol Spinal Rods in Conjunction with Titanium Pedicle Screws, *Mater. Sci. Eng. C*, 2017, **72**, p 601–610
14. P. Zhang, X.J. Liu, W.L. Lu, W.Z. Zhai, M.Z. Zhou, and J. Wang, Fretting Wear Behavior of CuNiAl Against 42CrMo4 Under Different Lubrication Conditions, *Tribol. Int.*, 2018, **117**, p 59–67
15. J. Geringer and D.D. Macdonald, Friction/Fretting-Corrosion Mechanisms: Current Trends and Outlooks for Implants, *Mater. Lett.*, 2014, **134**, p 152–157
16. F. Li, A.M. Wang, and C.T. Wang, Tribological Behavior of Articular Cartilage Against Medical Stainless Steel, *Tribology*, 2016, **36**, p 42–47
17. M. Fella, M. Labaiz, O. Assala, A. Lost, and L. Dekhil, Tribological Behavior of AISI, 316L Stainless Steel for Biomedical Applications, *Tribology*, 2013, **7**, p 135–149
18. H. Attar, K.G. Prashanth, A.K. Chaubey, M. Calin, L.C. Zhang, S. Scudino, and J. Eckert, Comparison of Wear Properties of Commercially Pure Titanium Prepared by Selective Laser Melting and Casting Processes, *Mater. Lett.*, 2015, **142**, p 38–41
19. C.R. Ramos-Saenz, P.A. Sundaram, and N. Difffoot-Carlo, Tribological Properties of Ti-Based Alloys in a Simulated Bone-Implant Interface with Ringer's Solution at Fretting Contacts, *J. Mech. Biomed. Mater.*, 2010, **3**, p 549–558
20. L. Vandenbulcke, M.I. Barros, C. Met, and G. Farges, Nano-Smooth Diamond Surfaces of Duplex Coatings on Titanium Alloy for Low Friction and Low Wear of Biomaterial Counterfaces, *Trans. Tech.*, 2002, **218–220**, p 595–600
21. A. Choubey, B. Basu, and R. Balasubramaniam, Tribological Behaviour of Ti-Based Alloys in Simulated Body Fluid Solution at Fretting Contacts, *Mater. Sci. Eng. A*, 2004, **379**, p 234–239
22. H. Li, D.B. Liu, Y. Zhao, F. Jin, and M.F. Chen, The Influence of Zn Content on the Corrosion and Wear Performance of Mg-Zn-Ca Alloy in Simulated Body Fluid, *J. Mater. Eng. Perform.*, 2016, **25**, p 3890–3895

23. D.B. Liu, B. Wu, X. Wang, and M.F. Chen, Corrosion and Wear Behavior of an Mg-2Zn-0.2Mn Alloy in Simulated Body Fluid, *Rare Met.*, 2015, **34**, p 553–559
24. L.B. Liu, D.B. Liu, Y.C. Liu, B. Wu, and M.F. Chen, Corrosion and Wear Behavior of Mg-x%Zn-0.8%Zr Alloy, *Rare Met. Mater. Eng.*, 2014, **43**, p 115–118
25. S.Y. Liu, J.W. Dai, S.N. Ni, Z.Z. Wang, and X.B. Zhang, Synergistic Effects of Wear and Corrosion on Mass Loss of GZ62 K Alloy in Simulated Body Fluid for Orthopedic Application, *Surf. Rev. Lett.*, 2018, <https://doi.org/10.1142/S0218625X19500215>
26. X.B. Zhang, J.W. Dai, H.Y. Yang, S.Y. Liu, X.C. He, and Z.Z. Wang, Influence of Gd and Ca on Microstructure, Mechanical and Corrosion Properties of Mg-Gd-Zn(-Ca) Alloys, *Mater. Technol.*, 2017, **32**, p 399–408
27. K. Chen, X.B. Zhang, J.W. Dai, Y. Fei, and Z.Z. Wang, Enhanced Mechanical and Corrosion Properties of NZ20K Alloy by Double Extrusion and Aging Processes for Biomedical Applications, *Mater. Technol.*, 2016, **31**, p 210–215
28. M.L. Hu, Q.D. Wang, C.J. Chen, D.D. Yin, W.J. Ding, and Z.S. Ji, Dry Sliding Wear Behaviour of Mg-10Gd-3Y-0.4Zr Alloy, *Mater. Des.*, 2012, **42**, p 223–229
29. W. Rong, Y. Zhang, Y.J. Wu, M. Sun, J. Chen, Y. Wang, J.Y. Han, L.M. Peng, and H.X. Ding, Effects of Zr and Mn Additions on Formation of LPSO Structure and Dynamic Recrystallization Behavior of Mg-15Gd-1Zn Alloy, *J. Alloys Compd.*, 2017, **692**, p 805–816
30. F. Labib, H.M. Ghasemi, and R. Mahmudi, Dry Tribological Behavior of Mg/SiC_p Composites at Room and Elevated Temperatures, *Wear*, 2016, **348–349**, p 69–79
31. Y. Liu, B. Jin, S. Shao, D.J. Li, X.Q. Zeng, and C.S. Xu, Dry Sliding Wear Behavior of Mg-Zn-Gd Alloy Before and After Cryogenic Treatment, *Tribol. Trans.*, 2014, **57**, p 275–282
32. A. Zafari, H.M. Ghasemi, and R. Mahmudi, Tribological Behavior of AZ91D Magnesium Alloy at Elevated Temperatures, *Wear*, 2012, **292–293**, p 33–40
33. A.J. López, P. Rodrigo, B. Torres, and J. Rams, Dry Sliding Wear Behaviour of ZE41A Magnesium Alloy, *Wear*, 2011, **271**, p 2836–2844
34. H.J. Hu, Z. Sun, Z.W. Ou, and X.Q. Wang, Wear Behaviors and Wear Mechanisms of Wrought Magnesium Alloy AZ31 Fabricated by Extrusion-Shear, *Eng. Fail. Anal.*, 2017, **72**, p 25–33
35. M. Sharifzadeh, M.A. Ansari, M. Narvan, R.A. Behnagh, A. Araee, and M.K.B. Givi, Evaluation of Wear and Corrosion Resistance of Pure Mg Wire Produced by Friction Stir Extrusion, *Trans. Nonferrous Met. Soc. China*, 2015, **25**, p 1847–1855
36. Y. Zong, G.Y. Yuan, X.B. Zhang, L. Mao, J.L. Niu, and W.J. Ding, Comparison of Biodegradable Behaviors of AZ31 and Mg-Nd-Zn-Zr Alloys in Hank's Physiological Solution, *Mater. Sci. Eng. B*, 2012, **177**, p 395–401
37. J.W. Dai, X.B. Zhang, Q. Yin, S.N. Ni, Z.X. Ba, and Z.Z. Wang, Friction and Wear Behaviors of Biodegradable Mg-6Gd-0.5Zn-0.4Zr Alloy Under Simulated Body Fluid Condition, *J. Magnes. Alloys*, 2017, **5**, p 448–453
38. L. Zhao, W. Chen, J.W. Dai, Z.Z. Wang, and X.B. Zhang, Effects of Heat Treatment on Corrosion and Wear Behaviors of Mg-6Gd-2Zn-0.4Zr Alloy in Simulated Body Fluid, *J. Mater. Eng. Perform.*, 2017, **26**, p 5501–5510